THE AC20.30 BLENDED WING BODY CONFIGURATION: DEVELOPMENT & CURRENT STATUS 2006

Dipl.-Ing. André Schmidt , Dipl-Ing. Hans Brunswig
HAW Hamburg, Fachbereich F+F

Berliner Tor 9, 20099 Hamburg, Germany

Abstract

The AC20.30 Blended Wing Body configuration was conceptualized and built at the HAW Hamburg to study next generation civil transports. New cabin concepts are being developed. The aerodynamics are studied on a 3.24m span flying model by comparison of data gained from CFD, wind tunnel and flight testing.

1   Introduction to the AC20.30

Due to the constantly rising number of passengers, high-volume civil transport aircrafts are needed in the future to relieve the limited airspace. The conventional tail plane concept has reached its limit with aircraft the size of the Airbus A380. The primary aerodynamic disadvantage of that concept is that the fuselage adds a significant amount of drag while contributing little to the lift.

Fig. 1:   AC20.30 approaching

So-called Blended Wing Body [BWB] aircrafts are a possible solution to overcome this drawback. BWBs are specifically designed to create a considerable part of the overall lift with their fuselage. Additionally, they offer an exceptional volume to carry payload. Thus, BWBs are expected to drastically decrease the cost of flying.

A student group researches a BWB concept entitled the AC20.30 (Fig. 1), which was conceptualized and built at the HAW Hamburg. The aims of the student project are:

- Basic research on next generation civil transports
- Flight testing theoretical solutions on a model scaled 1:30
- Detailed flight data and information on control of a BWB configuration gained through integrated measurement equipment
- Development of concepts for cabins for up to 900 passengers

Technical details of the AC20.30 model:

- wing span: $3.24m$
- length: $2.12m$
- take off mass: $12.5Kg$
- wing loading: $6.3Kg/m^2$
- engines: 2 electric impellers
- thrust: $2 \times 30N$
- power consumption: $2 \times 1.4KW$
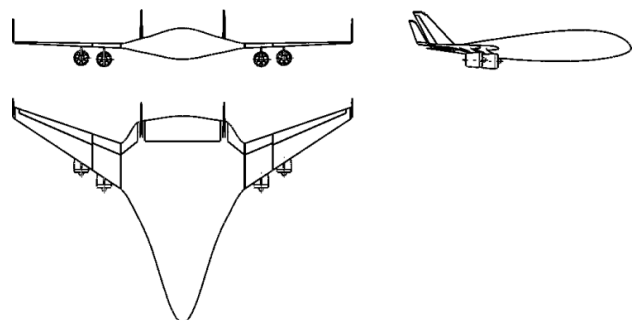
Fig. 2:   AC20.30 front, side and top view

The model can be divided into several structural components. The fuselage including its ribs and formers are made of an approximately 5mm thick glass fiber honeycomb core composite sandwich material. The wings and vertical tail planes are made of Styrofoam cores that are plated with wood and foil. The foil does not have any load carrying function, but serves only as waterproofing, aerodynamic cover and lastly, for aesthetic purposes. Winglets and nacelles are made of glass fiber.

Flight tests data-recording includes:
- side slip angle & angle of attack
- indicated airspeed
- turning rates and accelerations on all three axes
- temperature & pressure
- electrical power consumption
- height (QNH,QFE)
- rate of climb & rate of descent
- GPS

New cabin concepts
The Blended Wing Body fuselage design implies never before seen cabin dimensions. This calls for entirely new cabin concepts and evacuation procedures for up to 900 passengers.

The passengers' acceptance will be decisive if such a civil transport concept can ever be made reality. Therefore, the biggest challenges that have to be faced are the highest requirements on quality, ergonomics, design, handling, board service and logistics.

The student team works on innovative concepts and layout proposals. Concrete product designs are being developed in cooperation with supporting companies and other sponsors.

Aerodynamics
The aerodynamic properties of the AC20.30 are being investigated through conventional approaches: computational fluid dynamics, wind tunnel testing (chapter 2) and flight-testing.

The computation of flow around the AC20.30 is done primarily by utilizing the Boeing/NASA panel method Pan Air (a.k.a. A502i, chapter 3) and the computational fluid dynamics [CFD] code FLUENT (chapter 4). The results of both simulations will be compared to data gained from flight and wind tunnel testing.

2 Wind tunnel testing

In September 2005 wind tunnel tests were conducted on the flying AC20.30 model in the Göttingen-type open section low speed wind tunnel Dresden-Klotzsche (Fig. 3). During the test campaign the following parameters were set at wind speeds of $13m/s$ through $25m/s$:

- Angle of attack [AoA] $\alpha \in [0°;22°]$
- Elevator deflection $\eta_H \in [-20°;20°]$
- Aileron deflection $\eta_Q \in [-5°;20°]$
- Rudder deflection $\eta_S \in [-5°;20°]$
- Fuselage flap deflection $\eta_{K,R} \in [-5°;18°]$
- Wing flap deflection $\eta_{K,F} \in [-5°;20°]$

Fig. 3.   AC20.30 being mounted in the wind tunnel Dresden-Klotzsche

Technical data of the wind tunnel Dresden-Klotzsche:
- Nozzle width & height: $4.25m$ x $3m$
- Nozzle cross-section: $10m^2$ (quasi elliptical)
- Contraction ratio: 1:4.6
- Working section length: $5.25m$ to $8.25m$
- Max. power consumption: $1.35MW$
- Max. air speed: ca. $65m/s$
- Average turbulence: $< 0.5\%$

Due to the relatively wide span of the model compared to the wind tunnel's nozzle (76%), the raw test data has been adjusted to account for the downwash effect (Fig. 4).
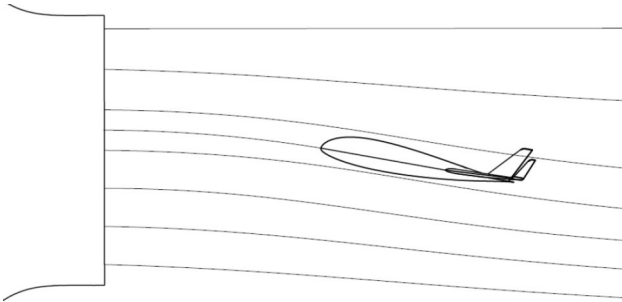
Fig. 4.   Downwash effect

The lift gradient (Fig. 5) shows a linear slope up until about $\alpha = 11°$, followed by a kink caused by the beginning flow separation on the wings. Nevertheless, the lift does not cease to increase in the measured range of AoAs until $\alpha = 21°$. In the high AoA regions the lifting body fuselage compensates for the loss of lift on the wings (in accordance with simulation results, see Fig. 13), showing a good stall behavior.
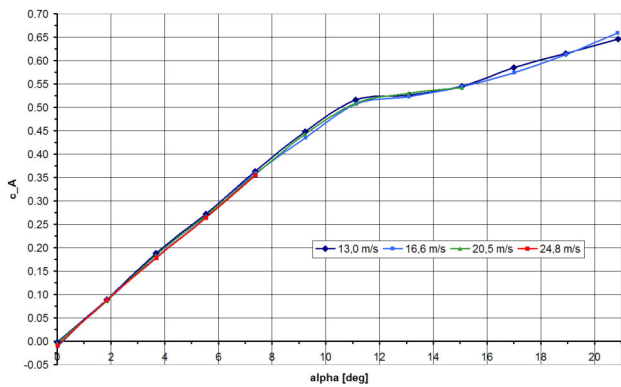
Fig. 5.   Lift gradient

Fig. 6 & Fig. 7 indicate an optimal AoA at about $\alpha = 9°$ with varying lift to drag ratios between eight and nine, depending on the air speed.

Fig. 8 shows a pitch moment coefficient in the CoG at $x_{C.G.} = 1.21m$. The negative, roughly linear slopes of the curves show pitch stability in the interval of $\alpha \in [0°;10°]$. The FLUENT

simulation (chapter 4) will show a stable behavior again at and above $\alpha = 18°$.

The wind tunnel results shall not be discussed in detail here. The interpretation will follow in conjunction with the simulation data in chapter 4.
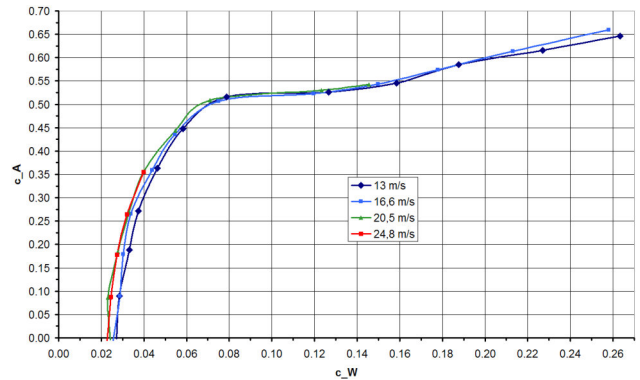
Fig. 6.   Drag polar
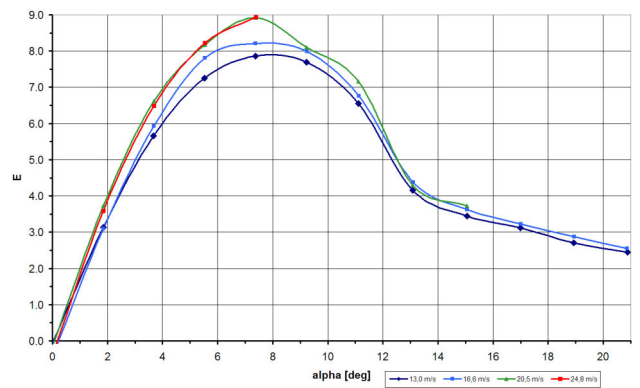
Fig. 7.   Lift to drag ratio
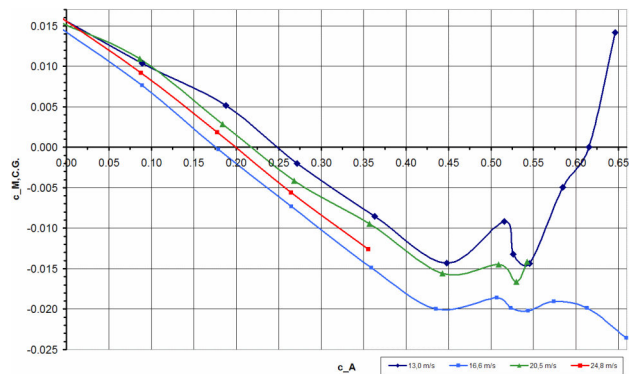
Fig. 8.   Pitch moment coefficient in the CoG over lift coefficient at 13m/s

3 Pan Air simulations

Pan Air is a numerical code using the potential theory equations. To compute a lifting body, it is modeled with quadrangular panels, similar to wire frame structures known from CFD or FEM models (Fig. 9).
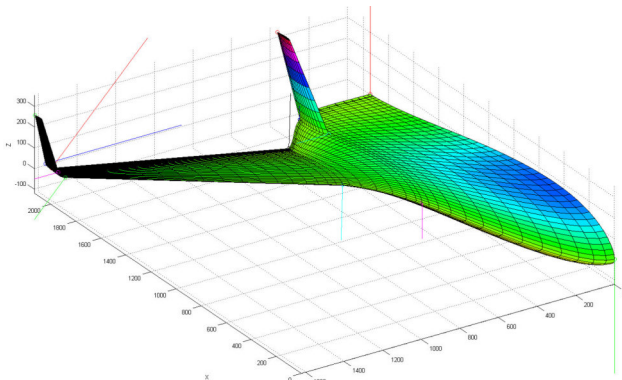
Fig. 9:   Panel model for the computation with Pan Air

Pan Air can compute arbitrary geometry without high requirements on the hardware. It, however, does not account for the effects of separated flow and friction.

Since the department does not own pre- or post-processing software for Pan Air, many simplifications were applied to the wire frame model when the AC20.30 was first conceived. At the time, it was not possible to factor in vertical surfaces, dihedral, curved wing edges or aerodynamic and geometric twist. The AC20.30-01 shows all of the above characteristics. Complex geometry like that simply could not be modeled with the tools at hand: Makewgs from the PDAS program package [5] and Wingwgs7 by Brabeck [2].

Recently, a considerable effort has been put into the coding of geometry conversion software. This software enables students to create arbitrary geometry with CAD (CATIA v5 in this case) and to translate it to a file format which is computable by Pan Air [6].

3.1 Grid generators

The use of so called grid generators or mashers is one possible method to transfer the AC20.30 CATIA model into a LaWGS grid (Pan Air input deck). Mashers allow taking CAD data, e.g.

an IGES surface model, and generating grid wires on the surfaces in the desired shape and resolution. The resulting scatter plot serves as geometrical input to the actual solver program.

3.1.1 AGPS

According Fliegel, Dickens & Winn [4] the programming language AGPS has been developed at Boeing during the past 20 years (as of 1998). It allows to write macros for the generation of complex geometry and to compile these in program packages. Highly sophisticated program libraries exist that make it possible even for non-experts to generate rather complex geometry with graphical tools as input decks for the panel codes A502 (Pan Air) and Transair.

Flaps, stabilizers, pylons, nacelles, etc. can be generated automatically with these AGPS tools. The source classifies a creation of these geometries by hand as extremely difficult and thus time consuming. As an example the program Fast502 is supposed to make the modeling of high lift systems possible in only a few days, as opposed to an effort of weeks and months by manual modeling. The Auto Paneling Package for CAD acts in similar ways as the newly developed tools presented in this article (section 3.2). Just like these, it requires a trimmed surface geometry without any overlaps and a gap tolerance value for Pan Air as input. The time saved for a fighter plane composed of 90 networks is said to be a few hours compared to several months by manual modeling. Furthermore, AGPS includes post-processing software to allow a graphical evaluation of the results, similarly to Panview (section 3.2).

The source states the volume of available macros to be some 300,000 lines of code. Unfortunately, the Department F+F of the HAW Hamburg does not hold licenses for the Boeing program libraries created with AGPS.

3.1.2 Gambit

However, the department does hold licenses for the masher Gambit. Gambit is the grid generator of the CFD code FLUENT. It allows the import and meshing of IGES models and other CAD input data.

A detailed CATIA model of the AC20.30 was exported as IGES and then meshed utilizing

Gambit. Gambit offers multiple options for storage of the generated grid data, depending on how the succeeding solvers require their input decks. These options include file formats for several FLUENT versions and other solvers. Unfortunately, none of these formats is the LaWGS format, which Pan Air requires as input.

3.2 Panview extensions

To allow the use of the Gambit-generated grids, new MatLab programs were written within the scope of Schmidt's thesis paper [6]. For user comfort, these programs were integrated into the then-current version of Panview.

Panview is a library of several MatLab programs, written by Beck [1] to allow for (graphical) evaluation of Pan Air output, and is thus considered a post processor. With the newly written code, Panview now incorporates a pre-processing part for geometric conversion, generation and assembly as well.
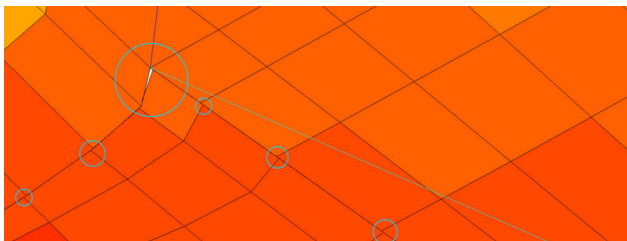
Fig. 10. Grid errors at network abutments

Grids generated with Gambit are saved using the so-called neutral format. The Panview extensions are able to convert these to LaWGS network by network.

Additionally, helper programs were written that allow turning over networks (the order of a network's point listing indicates to Pan Air which side of the network is outside/in the free stream). Other helper programs can fix errors occurring in Gambit at network abutments (Fig. 10). Still others are able to generate wing tips from arbitrary networks (Fig. 11).
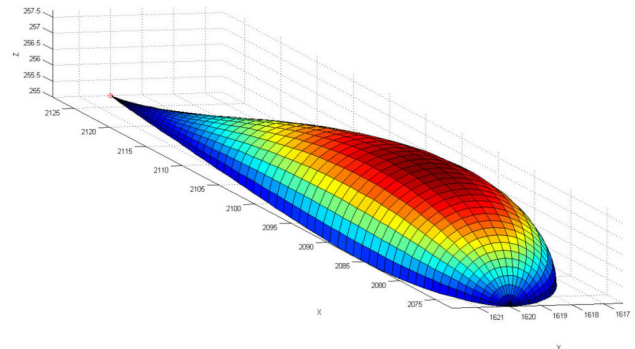
Fig. 11. Auto generated wing tip network (here 18 panels, respectively 10 degrees per panel, in circumferential direction)

3.3 Conclusion

Due to these enhancements to the Pan Air process it was possible to compute very detailed models of the AC20.30 consisting of over 5000 panels (Fig. 12). Aerodynamic properties at varying angles of attack and sideslip angles with and without winglets were examined.
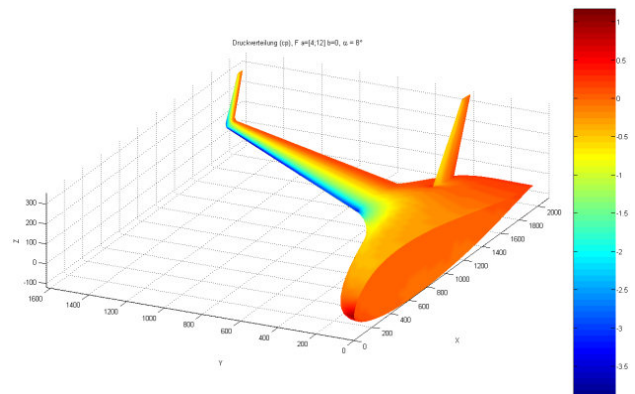
Fig. 12: Pan Air pressure distribution at 8 degrees AoA

Nevertheless, the simulation results gained with Pan Air will not be discussed here, as they are a very good match to the even more advanced FLUENT results, with the latter replacing the former.

4   FLUENT simulations

The behavior of the aircraft was also investigated in detail at different speeds and thrust settings using the Navier-Stokes based code FLUENT (Fig. 13). The information presented in

this chapter was adapted form Brunswig's thesis paper [**3**].
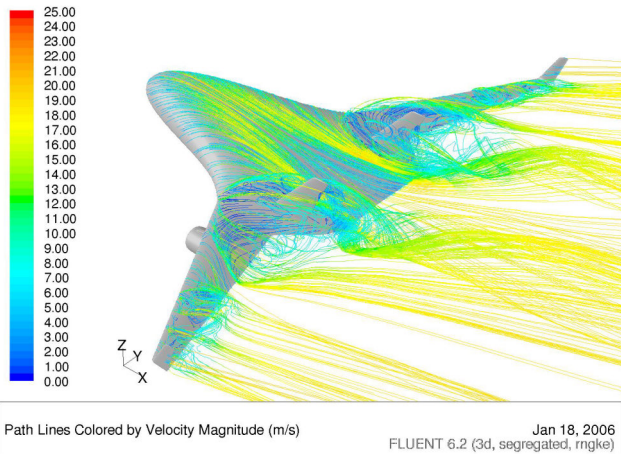
Fig. 13. Slip stream at 18 deg. AoA simulated with FLU-ENT

4.1 Lift

The lift gradients of the AC20.30 acquired by wind tunnel testing and CFD-simulation show an excellent match (Fig. 14). Pan Air and FLU-ENT show almost exact resemblance of the lift gradient $dc_A / d\alpha$, while the wind tunnel's lift curve slope is not quite as steep, as shown in the graph (about 4,8% difference). This slight divergence is based on the fact that the computational simulation assumes a perfect model, while the real model shows a number of disturbance-causing influences such as the nose boom, gaps between the control surfaces and the wings, actuator levers, inaccuracies in manufacturing etc..
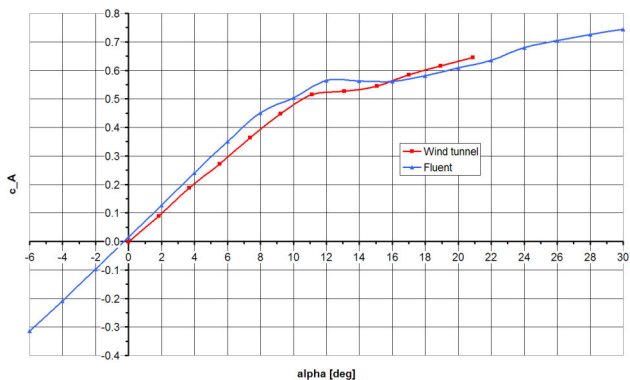
Fig. 14. Comparison of wind tunnel and CFD simulation lift gradients at 13m/s

$\alpha = 20°$
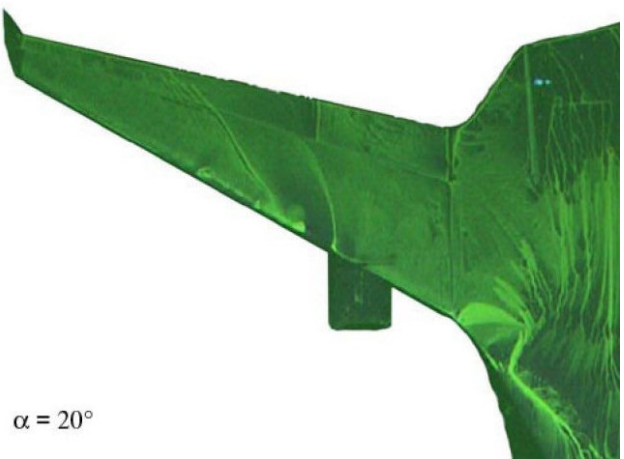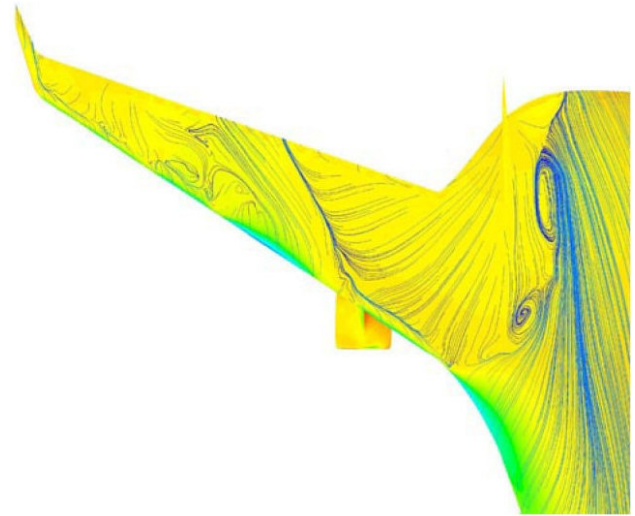
Fig. 15. Simulated surface stream lines (top) and in wind tunnel testing (bottom)

The first signs of separated flow show at $\alpha = 10°$ at the outer wing's trailing edge, as well as on the zenith wing surface in the area of the engine mounting. The dead water area on the zenith wing surface spreads with increasing AoA between engine and vertical stabilizer. At the same time the flow separates starting from the wing's trailing edge. In between those two areas there is a slim region where the air is able to follow the wing's contour up to $\alpha = 20°$. A good resemblance between wind tunnel testing and simulation is apparent in Fig. 15.

While the wing's flow is completely separated at high angles of attack, the flow on the fuselage does not separate within the investigated realm of up to $\alpha = 30°$, thus producing so much lift that a maximum AoA has not yet been reached. This phenomenon can be explained by

the relatively low local c_a-values. Also, energy rich flow streams up the fuselage and inward because of the fuselage's strong sweep. A stabilizing vortex generation as seen in high sweep delta wings or from strakes can not be detected, due to the absence of a sharp leading edge. The fact that the fuselage has such a big share in the overall lift generation underlines the distinctive BWB characteristics.

Nevertheless, AoAs that high cannot realistically be exploited within the flight envelope due to the separated flow on the wing's trailing edge, which results in the loss of all maneuverability of the elevons. The effective range of AoAs spans from 0 to 12 degrees.

4.2 Drag
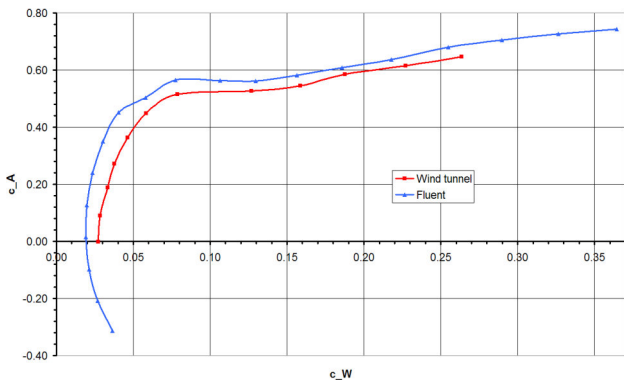
Fig. 16. Drag polars of FLUENT & wind tunnel at 13m/s
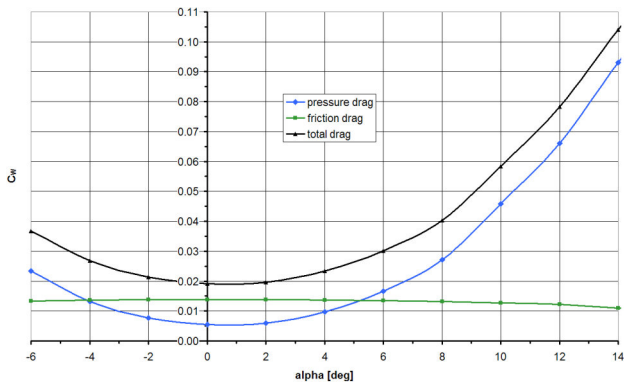
Fig. 17. Simulated drag components over AoA

The simulated and the empirical drag polars show only moderate accordance. Here, the differences between a perfect computer model and the as-built configuration of the AC20.30 add

up to show a drag that is too low and a lift assumed too high (see section 4.1).

At zero lift the share of friction drag is 71.6% of the total drag (Fig. 17). The share of the pressure drag rises with increasing AoA and shows the typical parabola shape of a drag polar. The friction drag is roughly constant at 0.0137 until $\alpha = 8°$. At higher AoAs it decreases due to the beginnings of flow separation and the therefore decreasing wetted surface area. The shear stress distribution on the surface supports this (Fig. 18).
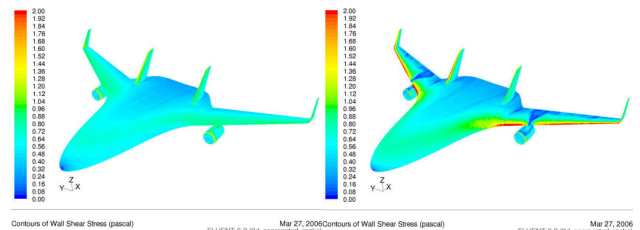
Fig. 18. Wall shear stress at 0 (left) & 10 (right) deg. AoA

Since the FLUENT simulation shows higher lift and lower drag coefficients the lift to drag ratio strongly varies from the test data (Fig. 19). While the wind tunnel measurements indicate optimal lift to drag ratios of 7.9 to 8.9 (depending on the speed) at $\alpha = 8°$, the simulation returns values of 11.6 to 12.5 at $\alpha = 6°$.

At first sight, both sets of values seem rather small compared to common civil transport aircraft with lift to drag ratios of about 20. This is especially true considering a good lift to drag ratio is expected to be one of the big advantages of BWB configurations. It has to be taken into account, though, that the subject under investigation is a model aircraft equipped with adequate airfoils, flying at low subsonic speeds. The lift to drag ratio increases with accelerated speeds. The boundary layer becomes thinner, which leads to a lower pressure drag share. The increase of speed from 13m/s to 20m/s already results in an increase of the lift to drag ratio of 7.7% in the simulation and 12.7% in the empirical data.
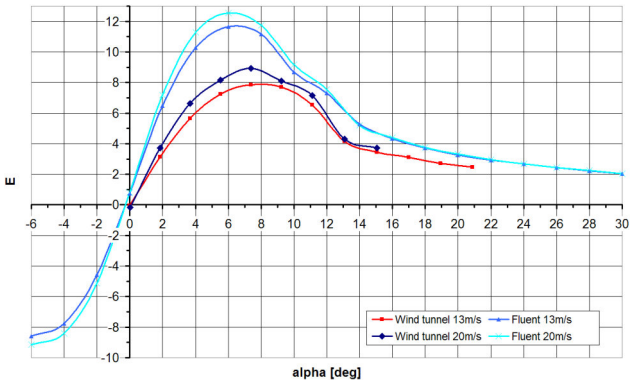
Fig. 19. Comparison of lift to drag ratios

4.3 Engine thrust
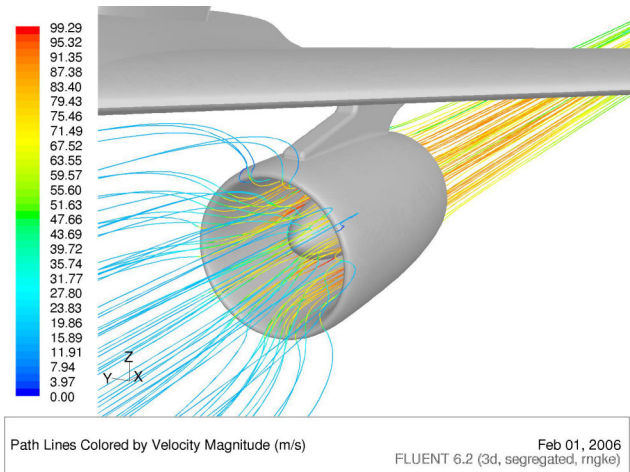
Fig. 20. Engine streamlines at 13m/s, zero AoA and full thrust

The engines were tested in the wind tunnel using three different thrust levels: 7, 20 & 29N per engine. In FLUENT, the engine thrust is modeled by a step function in pressure, calibrated to reach the thrust values of the wind tunnel tests at zero air speed. The influence of the engines is investigated at $\alpha \in [0°; 8°]$ and for wind speeds of 13 and 20m/s, thus resulting in 24 simulations (Fig. 20).

The net thrust decreases with increasing air speed (Fig. 21). Overall, the simulation shows lower thrust values than the tests at increasing air speeds.
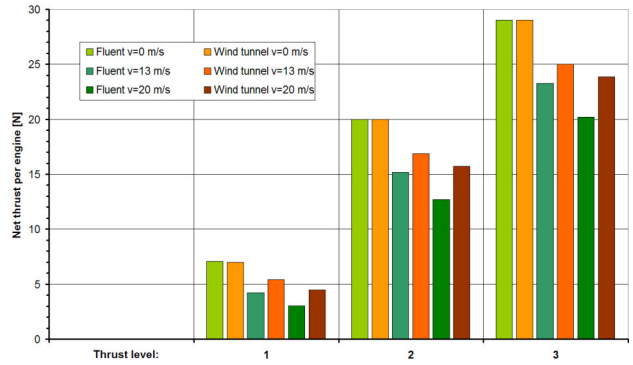
Fig. 21. Net thrust per engine at varying air speeds

As seen in Fig. 14, the lift curve slope of the test is slightly lower than the one of the simulation (Fig. 22). The engines' thrust causes the slope to increase. At $\alpha = 0°$ the lift is decreased by the accelerated air on the wings' nadir side. At AoAs above about 4.5 degrees the thrust vector in lift direction causes the lift coefficient to supersede the unpowered coefficient.
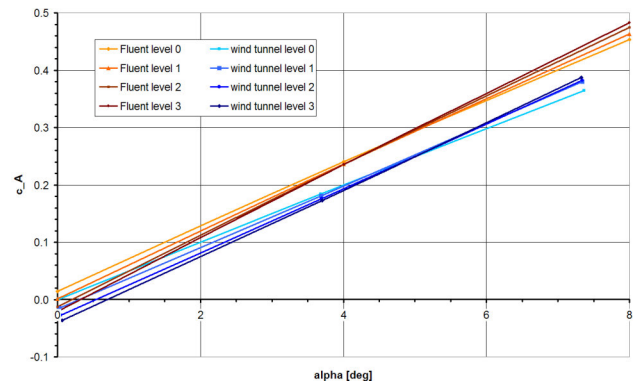
Fig. 22. Lift gradients at different thrust levels at 13m/s

Naturally, the thrust decreases the measurable drag. At 13m/s thrust level 1 suffices to overcome the drag (Fig. 23). At 20m/s level 2 is required already.
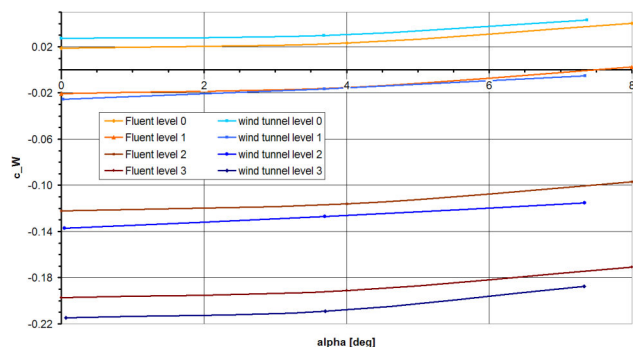
Fig. 23. Drag over AoA at different thrust levels at 13m/s

Also, the pitch moment is influenced by the engines' thrust. Due to their mounting position on the wings' nadir side, the thrust causes a pitch up moment (Fig. 24).
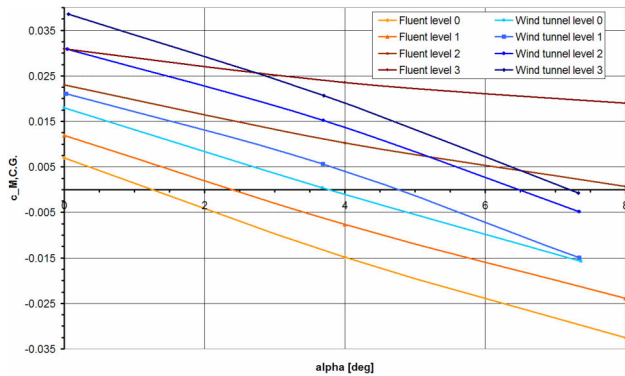
Fig. 24. Pitch moment over AoA at different thrust levels at 13*m/s*

5   Conclusion

In the past year the aerodynamic characteristics of the AC20.30 BWB configuration were extensively researched. Theoretical data was gained by simulation with Pan Air and FLUENT as well as experimental data from wind tunnel experiments. These data sets supplement the results previously obtained through flight testing.

In the future all data sets must reach a common denominator, to create a comprehensive understanding of the aerodynamic properties of this BWB configuration.

6   Nomenclature

Roman

AGPS	Aero Grid and Paneling System geometry language
AoA	Angle of Attack
c	coefficient
CAD	Computer Aided Design
CFD	Computational Fluid Dynamics
CoG	Center of Gravity
BWB	Blended Wing Body
E	lift to drag ratio
FEM	Finite Elements Method
IGES	Initial Graphics Exchange Specification
LaWGS	Langley Wireframe Geometry Standard
PDAS	Public Domain Aeronautical Software

Greek

α	angle of attack
η	angle of deflection

Indices

a	local (airfoil) lift
A	lift
C.G.	center of gravity
F	wing
H	elevator
K	flap
M	moment
Q	aileron
R	fuselage
S	rudder
W	drag

7   References

[1] Beck N. *Untersuchung der Umströmung von Pfeilflügeln mit einem Paneelverfahren*, Hamburg, HAW Hamburg, Fachbereich Fahrzeugtechnik & Flugzeugbau, Diplomarbeit, 2002

[2] Brabeck N. *WINGWGS7*, Hamburg, FH Hamburg, Fachbereich Fahrzeugtechnik & Flugzeugbau, 2001

[3] Brunswig H. *Bestimmung der aerodynamischen Eigenschaften des BWB-Modells AC20.30 mit Methoden der CFD*, Hamburg, HAW Hamburg, Fachbereich Fahrzeugtechnik & Flugzeugbau, Diplomarbeit, 2006

[4] Fliegel D., Dickens T. and Winn A. *Experience With a Geometry Programming Language for CFD Applications*, 98WAC-56, The Boeing Company, Society of Automotive Engineers, Inc., 1998

[5] PDAS: *Public Domain Aeronautical Software*, [http://pdas.com/]

[6] Schmidt A. *Berechnung der Strömung einer Blended-Wing-Body-Konfiguration mit dem Paneelverfahren Pan Air*, Hamburg, HAW Hamburg, Fachbereich Fahrzeugtechnik & Flugzeugbau, Diplomarbeit, 2005